Novel phosphorus-containing halogen-free ionic liquid toward fire safety epoxy resin with well-balanced comprehensive performance

Yue-Quan Shi, Teng Fu, Ying-Jun Xu, De-Fu Li, Xiu-Li Wang, Yu-Zhong Wang

PII: S1385-8947(18)31490-6
DOI: https://doi.org/10.1016/j.cej.2018.08.023
Reference: CEJ 19637

To appear in: *Chemical Engineering Journal*

Received Date: 16 April 2018
Revised Date: 24 July 2018
Accepted Date: 4 August 2018

Please cite this article as: Y-Q. Shi, T. Fu, Y-J. Xu, D-F. Li, X-L. Wang, Y-Z. Wang, Novel phosphorus-containing halogen-free ionic liquid toward fire safety epoxy resin with well-balanced comprehensive performance, *Chemical Engineering Journal* (2018), doi: https://doi.org/10.1016/j.cej.2018.08.023

Novel phosphorus-containing halogen-free ionic liquid toward fire safety epoxy resin with well-balanced comprehensive performance

Yue-Quan Shi, Teng Fu, Ying-Jun Xu, De-Fu Li, Xiu-Li Wang*, Yu-Zhong Wang

Center for Degradable and Flame-Retardant Polymeric Materials, College of Chemistry, State Key Laboratory of Polymer Materials Engineering, National Engineering Laboratory of Eco-Friendly Polymeric Materials (Sichuan), Sichuan University, Chengdu 610064, China.

*E-mail address: xiuliwang1@163.com

Fax: +86-28-85410755; Tel: +86-28-85410755

ABSTRACT

Most flame retardants used in epoxy resin (EP) inevitably affect its curing process, mechanical properties as well as transparency. To solve this problem, a novel phosphorus-containing halogen-free ionic liquid ([Dmim]Tos), composed of imidazole cation modified with 9,10-dihydro-9-oxa-10-phosphaphenanthrene-10-oxide (DOPO) and tosylate anion, has been designed and used as a flame retardant for EP. DSC non-isothermal curing scans show that [Dmim]Tos has accelerating effect on the curing of EP. The addition of [Dmim]Tos enhances not only the crosslinking density but also the modulus of EP. The unnotched izod impact strength and the glass transition temperatures (T_gs) of EP/[Dmim]Tos are a little lower than pure EP because of the plasticization of unreacted [Dmim]Tos. Due to the good affinity with epoxy

resin, low [Dmim]Tos addition almost has no effect on the the transparency of EP. Besides, incorporation of 4 wt% [Dmim]Tos into EP makes it pass UL-94 V-0 level and increases the LOI value to 32.5%. Cone calorimeter test indicates the peak heat release rate (*p*-HRR) of EP/4.0[Dmim]Tos reduces by 37% compared with EP. The flame-retardant mechanism of EP/[Dmim]Tos has been investigated in detail. It is found that the flame-retardant action of [Dmim]Tos on EP is in the gas phase for quenching effect of phosphorus-based radicals and the condensed phase for dehydration of phosphorous fragments.

Keywords: Ionic liquid; DOPO; Epoxy resin; Flame retardance; Curing; Mechanical properties

1. Introduction

Epoxy resin (EP), one of the most important thermoset resins, has been widely used in various fields such as coatings, adhesives, composites, laminates, electronic insulators, etc., owing to its low cost, easy fabrication, excellent moisture, chemical resistance and attractive mechanical properties [1-3]. However, the high flammability of EP restricts its wider applications in many areas. So, it is urgent to endow EP with flame retardancy especially when it is used in the areas requiring high fire resistance.

Usually a flame retardant can be added into the epoxy matrix, either as a reactive co-reactant or an additive, which has demonstrated as an efficient method [4-6]. Unfortunately, the thermal stability, the glass transition temperature (T_g) as well as the mechanical properties of EP are sacrificed as a cost for the flame retardancy [7-9].

Sometimes, the curing process is also affected, presented as higher curing temperature and longer curing time [10]. How to balance the flame retardancy and the comprehensive properties of EP still is a challenge [11].

Ionic liquids (ILs) are known as the most promising solvents and catalysts in 21st century due to their wide liquid range, high conductivity, negligible vapor pressure, low flammability and wide electrochemical potential window [12-16]. In the last decade, ILs have been investigated as lubricants [17], plasticizers [18], antistatic agents [19], compatibilizer [20] etc., for polymeric materials. Let alone, they have been extensively used as solvents for indissolvable biomacromolecules [21-24].

In addition to the application above, ILs have also been studied in the field of flame retardance. For example, there are some literatures reporting that ILs with special structure can be applied as synergists to endow different kinds of polymeric materials with flame retardancy [25-28]. For example, a phosphrous-containing ionic liquid ([PCMIM]Cl) has been synthesized by Yang et al. and used together with ammonium polyphosphate (APP) to constitue a intumescent flame retardant (IFR) for polypropylene (PP) [27]. It is found that [PCMIM]Cl has an obvious synergistic effect with APP, resulting in that PP/IFR reaches UL-94 V-0 rating and has a limiting oxgen index (LOI) of 31.8%, when the total amount of IFR is 30 wt%. Li et al. [28] has designed a kind of polyoxometalates-based ionic liquid (PIL) and also has introduced into PP/IFR system to investigate its synergistic effect on the thermal and flame retardant properties of PP. Their results show that PP composite with 14.5wt% IFR and 0.5wt% PIL passes UL-94 V-0 rating, presenting better flame retardant efficiency

than that of single IRF. But it is rare to use IL alone as a flame retardant for polymers in the currrent study. Xiao et al. has synthesized a phosphonate-based imidazolium bromide ionic liquid, and used alone as a flame retardant for epoxy resin [29]. With only 4 wt% loading, EP/IL has the LOI value of 34.9% and passes UL-94 V-0 rating. However, this IL contains bromide anion, and it will release toxic and corrosive products during combustion just like those halogen flame retardants [30].

It has been well demonstrated that N-methyl imidazole can be used as a latent curing agent for EP, indicating it has good compatibility with EP [31]. So, it provides a possibility to design a kind of imidazole ionic liquid that contains flame retardant element, which can endow EP with better flame retardancy without affecting its curing behavior and other properties. In addition, based on our previous results [32], ILs with sulfate anions are not only non-toxic, but also make contribution to flame retardancy. It has been well demonstrated that 9,10-dihydro-9-oxa-10-phosphaphenanthrene-10-oxide (DOPO) or its derivatives as phosphorus-containing flame retardants, exhibit excellent thermal stability and flame retardancy compared with other phosphorus-based flame retardants [33-35]. Therefore, in this study, we design a novel flame-retardant IL containing imidazole modified with DOPO as a cation and sulfate as an anion. The comprehensive performances of EP containing this IL, including flame retardance, curing behavior, transparency, mechanical properties and thermal stability, have been investigated. The flame retardant mechanism is also discussed by the analysis of pyrolysis products and char layer.

2. Experimental section

2.1. Materials

Epoxy resin of diglycidyl ether of bisphenol A (DGEBA, E-44) with epoxy value of 0.41-0.47 mol/100 g, was purchased from Lanxing Resin Co., Ltd (Lanzhou, China) and used as received. 9,10-Dihydro-9-oxa-10-phosphaphenanthrene-10-oxide (DOPO) was supplied by Jinlong Chemical Technology Co (Shenzhen, China). 4,4-Diaminodiphenyl methane (DDM) was purchased from Sinopharm Chemical Reagent Co., Ltd. (Shanghai, China). Para-toluenesulfonyl chloride (TosCl) was provided by Tianjin BoDi Chemical Ind. Co. Ltd. (Tianjin, China). Acetonitrile, triethylamine, dichloromethane, diethyl ether, acetone and ethanol were all supplied from KeLong Chemical Reagent Co., Ltd (Chengdu, China) and used as received.

2.2. Synthesis of (6-oxidodibenzo[c,e][1,2]oxaphosphinin-6-yl)methyl 4-methylbenzenesulfonate (DOPO-Tos)

DOPO-OH (123 g, 0.5 mol, prepared according to the literature [36]), trimethylamine (50.9 g, 0.5 mol) and 200 mL dichloromethane were added into a 500 mL four-neck flask equipped with a mechanical stirrer, additional funnel, and reflux condenser. 90 g (0.5 mol) paratoluensulfonyl chloride was added slowly into the flask after the mixture becoming a homogenous turbid solution. The reaction was maintained at room temperature for 6 h, and then the mixture was washed with the hot ethanol. Finally, the obtained product was dried at 80 °C in vacuum oven for 10 h. The yield of the product

was 85%. ^{1}H-NMR (400 MHz, δ_H, DMSO-d_6, ppm): 4.05 (t, 3H), 4.76 (t, 1H), 5.02 (m, 1H),7.14~7.25 (m, 1H), 7.26~7.40 (m, 3H), 7.40~7.62 (m, 4H), 7.80~7.94 (m, 2H), and 8.15~8.30 (m, 2H). The ^{1}H NMR spectrum of DOPO-Tos is shown in Fig. S1.

2.3. Synthesis of 1-methyl-3-((6-oxidodibenzo[c,e][1,2]oxaphosphinin-6-yl)methyl)-1H-imidazol-3-ium 4-methylbenzenesulfonate ([Dmim]Tos)

The obtained DOPO-Tos (59.8 g, 0.15 mol) was dissolved into 80 mL N-methylimidazole in 250 mL flask at 80 °C and maintained stirring for 48 h. The product [Dmim]Tos was obtained by precipitation after washing with acetonitrile and diethyl ether, respectively. Finally, the product dried at 80 °C in vacuum to a constant weight. The corresponding synthetic routes for DOPO-Tos and [Dmim]Tos are shown in Scheme 1. The total yield of [Dmim]Tos was 60%. The chemical structure of [Dmim]Tos was confirmed by ^{1}H-NMR, ^{13}C-NMR, ^{31}P-NMR and ESI-MS. ^{1}H-NMR, (400 MHz, δ_H, DMSO-d_6, ppm): 9.1 (s, 1H), 8.7 (s 1H), 6.8~8.4 (m, 14H), 5.4 (m, 2H), 3.8 (d, 3H), and 2.3 (s, 3H). ^{13}C-NMR, (400 MHz, δ_H, D_2O, ppm): 152.3 (C^4), 141.2 (C^{11}), 135.8 (C^{12}), 133.1 (C^5), 132.5 (C^7), 131.9 (C^{10}), 131.2 (C^8), 129.8 (C^{14}), 129.0 (C^9), 127.8 (C^6), 123.0 (C^{16}), 120.3 (C^{15}), 116.2 (C^{13}), 50.0 (C^3), 49.0 (C^2), and 35.8 (C^1). ^{31}P-NMR, (400 MHz, δ_H, DMSO-d6, ppm): 12.2 (s). ESI-MS (40 eV): $[M+NH_3]^+$ calculated: 499.14, found: 499.10.

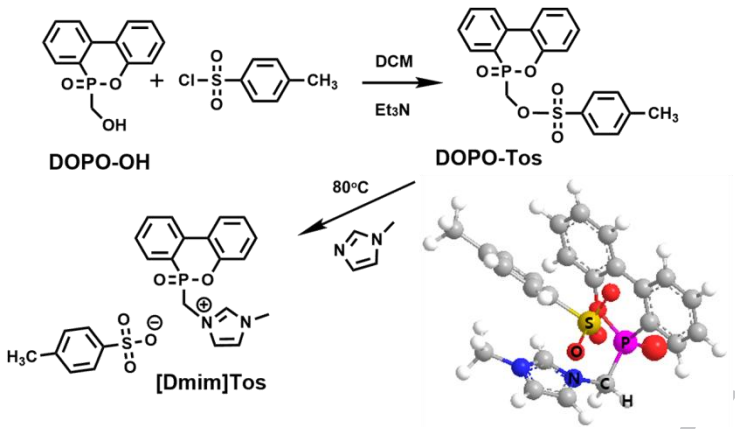

Scheme 1. Synthetic route for [Dmim]Tos and 3D structure of [Dmim]Tos obtained by Chembio 3D MM2 Minimize Energy.

2.4. Curing of EP and EP/[Dmim]Tos

The cured EP and EP/[Dmim]Tos samples were prepared through traditional curing process, in which DDM was chosen as a curing agent. The detailed preparation process for cured EP is described as follows: DGEBA (100 g) and different amount of [Dmim]Tos were first mixed together and stirred at 100 °C until [Dmim]Tos was completely dissolved in DGEBA. Then, the mixture was placed in vacuum until no bubbles emerged. DDM was fed into the mixture at 80 °C, and maintained stirring and vacuum for 3 min. Finally, the mixture was poured rapidly into a preheated mold and thermally cured at 120 °C for 3 h, and postcured at 150 °C for 2 h. The EP sample was cured by the same procedure without the addition of [Dmim]Tos. The samples were named as EP, EP/2.4[Dmim]Tos, EP/4.0[Dmim]Tos, EP/7.5[Dmim]Tos respectively, in which the number denoted the weight percentage of [Dmim]Tos in EP.

2.5. Characterization

^{1}H-NMR (400 MHz), ^{31}P NMR (161.9 MHz) and ^{13}C NMR (100 MHz) spectra were obtained on a Bruker Avance III 400 spectrometer (Rheinstetten, Germany). For ^{1}H NMR (400 MHz) and ^{31}P NMR (161.9 MHz), d6-dimethyl sulphoxide (DMSO) was used as a solvent. D_2O was used as a solvent for ^{13}C NMR (100 MHz). TMS was used as an internal reference for ^{1}H NMR.

ESI-MS spectra was obtained by a LCMS-IT-TOF spectrometer (Shimadzu, Japan) using water as a solvent.

Thermogravimetry analysis (TG) was performed on a TG 209F1 apparatus (NETZSCH, Germany). The samples (5.0±0.5 mg) were heated from 40 °C to 700 °C at a rate of 10 °C min^{-1} under nitrogen or air flow of 50 mL min^{-1}.

Scanning electronic microscopy (SEM, Phenom Pro V, Holland) was utilized to observe the morphology of residues after cone calorimeter test and the cryo-fractured surface of different samples at an accelerating voltage of 10 kV. The elemental analysis was conducted by the energy dispersive X-ray spectrometer (EDX) in the surface scanning model. All samples were coated with gold prior to the SEM observation.

DSC was carried on a TA Q200 DSC (TA, USA) equipped with a thermal analysis data station at a heating rate of 10 °C·min^{-1} under N_2 atmosphere.

The cone calorimeter (cone) was performed to analysis the combustion behavior of the samples with a FIT (UK) cone calorimeter according to ISO 5660-1. The samples with the size of 100×100×3 mm^3 were measured under a heat flux of 35 kW

m^{-2}. The average values of each sample were obtained from at least four measurements, and the experiment error was about ± 10%.

The limited oxygen index (LOI) of the samples was evaluated by a HC-2C oxygen index meter (Jiangning, China) and the sheet dimensions was 130 mm × 6.5 mm × 3.2 mm according to ASTM D2863-97. The vertical burning test (UL-94) for the samples with the size of 130 mm × 13mm × 3.2 mm was carried out by a vertical burning instrument (CF-2) according to ASTM D3801. The results of each samples were obtained from at least five measurements.

Pyrolysis-gas chromatography/mass spectrometry (Py-GC/MS) was carried out using a DANI MASTER GC-TOF-MS systems (DANI, Italy) combined with a CDS5200 pyrolyzer (CDS, America). The samples were heated from ambient temperature to 350°C at a rate of 1000 °C/s in helium atmosphere with an isothermal step of 20 s. The heating program of the capillary column was as follows: the temperature was maintained at 45 °C for 2 min, then increased to 280 °C at a rate of 15 °C/min and kept at 280 °C for 5min. The data of mass spectra were analyzed using the NIST library.

Raman spectra were obtained on a LabRAM-HR Confocal Raman Microprobe (JobinYvon Instruments, France) with a 512.5 nm argon ion laser.

X-ray photoelectron spectroscopy (XPS) spectra were recorded by a XSAM80 apparatus (Kratos Co, UK), using Al Kα excitation radiation (hν =1486.6 eV).

Dynamic mechanical analysis (DMA) was tested in a three point bending pattern using a DMA Q800 apparatus (TA instruments). The testing conditions were set as

follows: constant frequency = 1.0 Hz, oscillation amplitude = 10.0 μm, heating rate = 10 °C min^{-1}.

Izod unnotched impact strength was measured in ISO 180:2000 (Plastics-Determination of Izod impact strength) with a dimensional size of 78 mm × 8 mm × 4 mm. Commercial tensile tester (INSTRON 3366, USA) was used to test the tensile properties of samples according to GB/T1040.3-2006 at a speed of 1 mm/min with a dumbbell-shaped samples size of 25 mm × 4 mm × 2 mm. At least five specimens were tested for each sample, and the typical results was reported.

3. Results and discussions

3.1. Structure characterization of [Dmim]Tos

As shown in Scheme 1, [Dmim]Tos can be synthesized through the reaction of quaternization between N-methylimidazole and sulfonate [32]. As shown in Fig.1, The signals at 9.1 ppm, 8.7 ppm and 7.6 ppm in the ^{1}H-NMR spectrum are assigned to the H^{1}, H^{2} and H^{3} of N-methylimidazole, respectively. The chemical shift of methyl in imidazole ring (H^{4}) appears at 3.8 ppm. The chemical shifts of protons belonged to DOPO can be found in the range of 6.8~8.4 ppm [37]. Besides, the chemical shifts at 7.4 ppm, 7.1 ppm, 2.3 ppm are ascribed to H^{7}, H^{8}, H^{6} of *p*-toluene sulfonate anion.

Additionally, all the characteristic carbon resonance peaks of [Dmim]Tos can be found in its ^{13}C-NMR spectrum. The carbon resonance peaks derived from DOPO are found in the range of 116-136 ppm. The carbon signals of N-methylimidazole appear at 49.0 (C^{2}), 152.3 (C^{4}), 133.1 (C^{5}) and 127.8 (C^{6}) ppm. The carbon resonance peaks

which belong to *p*-toluene sulfonate anion, appear at 35.8 (C_1), 131.2 (C_8), and 132.5 (C_7) ppm. There is only a single peak for ^{31}P NMR spectrum at 12.2 ppm, demonstrating only one type of phosphorus in [Dmim]Tos. To further investigate the structure of [Dmim]Tos, We use ESI-MS to measure the molecular weight of [Dmim]Tos. It is found that the maximum absorption peak of [Dmim]Tos is at 499.10, which is as same as the calculated value of 499.14 $[M+NH^3]^+$. All the above results demonstrate that [Dmim]Tos has been successfully synthesized.

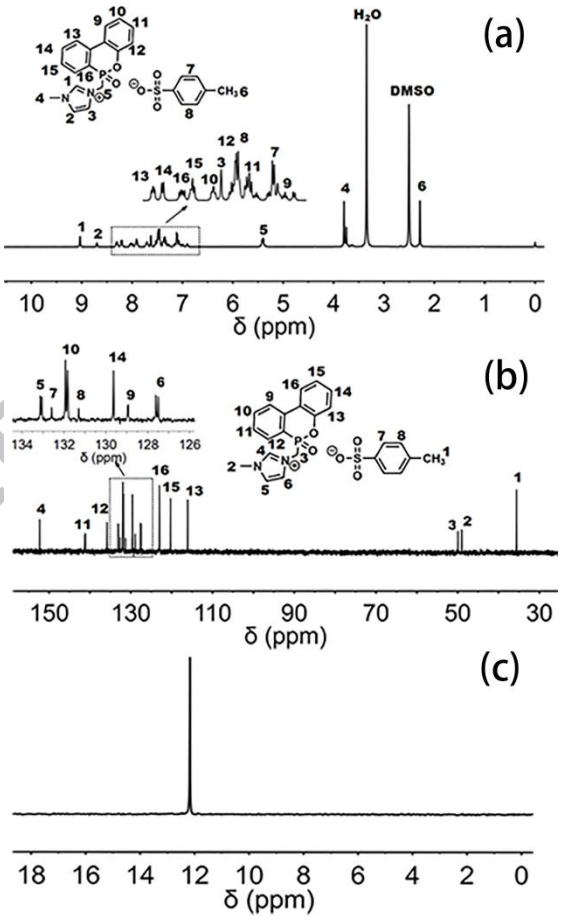

Fig. 1. ^{1}H-NMR (a), ^{13}C- NMR (b), ^{31}P-NMR (c) spectra of [Dmim]Tos.

3.2. Curing behavior and mechanical properties of EP/[Dmim]Tos

To find how [Dmim]Tos affects the curing behavior of EP, non-isothermal curing scans of EP with different amount of [Dmim]Tos have been investigated by DSC. The DSC heating curves of EP/[Dmim]Tos and the consumption of epoxy resin at different amount of [Dmim]Tos are shown in Fig. 2. From the DSC heating curves, we can see that the maximal exothermic temperatures of EP/[Dmim]Tos become lower with the increase of [Dmim]Tos. Besides, the consumption of EP/[Dmim]Tos at different temperature is higher than that of pure EP. And the consumption of EP/[Dmim]Tos at the temperature range of 120-150 °C, which is consistent with the practical curing temperature, is linearly increased with the loading of [Dmim]Tos. These results indicate that [Dmim]Tos has accelerating effect on the curing process of EP. This phenomenon is different with that reported flame retardants used in EP, which will delay the curing process of EP, reflected by the higher curing temperatures and longer curing time [10]. It is well known that imidazole and its derivatives can be used as a latent curing agent for EP [38-40], due to the acid and basic properties caused by the nitrogen atom in imidazole ring. For [Dmim]Tos, parts of the substituted imidazole also can react with DGEBA to form an adduct, which will further initiate the polymerization of diglycidyl ether [41, 42]. Therefore, the curing process of epoxy resin is accelerated when [Dmim]Tos is added.

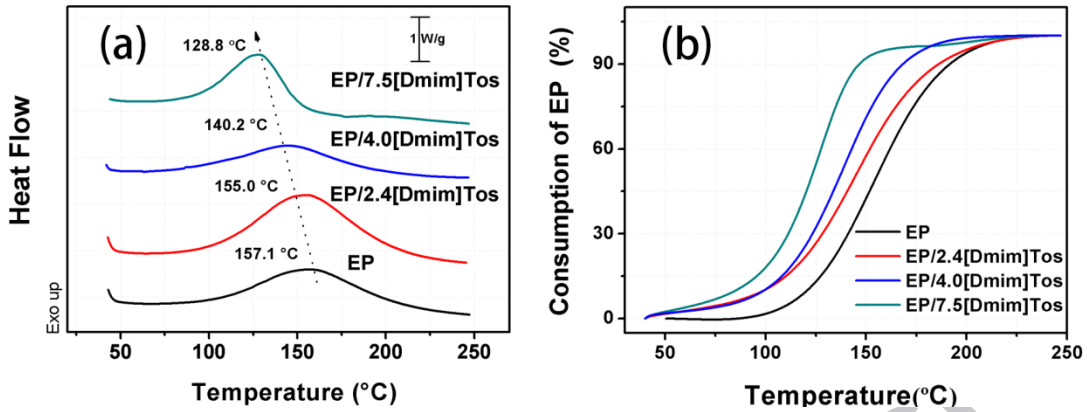

Fig. 2. DSC heating scans of EP and EP/[Dmim]Tos (a), and the consumption of EP at different loading of [Dmim]Tos (b).

To further demonstrate this, DMA is used to determine the crosslinking density of EP thermosets. Fig. 3 shows the storage modulus and tan delta curves of different samples. According to the literature, the crosslinking density of the EP (ν_e) can be calculated by the rubber elasticity theory [43, 44] with the Eq. (1)

$$\nu_e = E'/3RT \qquad (1)$$

where E′ is the storage modulus at T_g + 40 °C in the rubbery plateau, R is the ideal gas constant, T is the thermodynamic temperature at T_g + 40 °C, and T_g is obtained from the peak temperature of tanδ in Fig. 3. The obtained values of ν_e are listed in Table 1. From the Table 1, we can see clearly that the crosslinking density of all EP/[Dmim]Tos is raised compared to pure EP. In addition, the crosslinking density of EP/[Dmim]Tos is almost linearly increased with the increase of [Dmim]Tos loading. This result means that the degree of crosslinking of EP/[Dmim]Tos is denser compared to the pure EP, demonstrating that [Dmim]Tos participates the curing processing of EP.

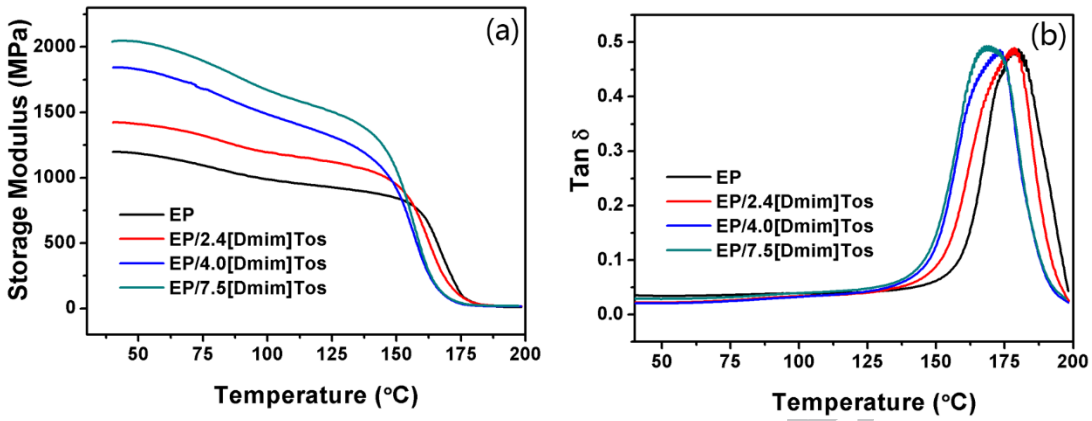

Fig. 3. DMA curves of EP and EP/[Dmim]Tos.

Table 1 Mechanical properties, T_g, and crosslinking density (ν_e) of EP and EP/[Dmim]Tos.

Samples	Stress at break (MPa)	Elongation at break (%)	Young Modulus (MPa)	T_g^a (°C)	T_g^b (°C)	Storage modulus at 50 °C (MPa)	ν_e (mol/m^3)
EP	77.1±3.2	8.4±0.4	1232±40	181.6	143.7	1184	822.5
EP/2.4[Dmim]Tos	78.4±1.0	8.6±0.6	1421±35	180.4	138.1	1410	1276.7
EP/4.0[Dmim]Tos	68.4±1.1	8.2±0.3	1393±32	173.6	139.6	1828	1445.2
EP/7.5[Dmim]Tos	64.2±2.7	7.9±0.9	1491±85	170.4	138.7	2040	1636.7

a: determined by DMA; b: determied by DSC

The storage modulus of EP/[Dmim]Tos is much higher than that of EP when the temperature is below 150 °C (Fig. 3a), illustrating the rigidity of EP/[Dmim]Tos is enhanced. This phenomenon can be ascribed to the higher crosslinking density and the rigid DOPO structure in [Dmim]Tos [45]. Generally, the enhanced crosslinking density should increase the T_gs of EP/[Dmim]Tos. But as shown in Table 1, the T_gs of EP/[Dmim]Tos determined by DMA or DSC (Fig. S2) slightly decrease compared with EP. This result means not all [Dmim]Tos participates the curing reaction, the residual ionic liquid acts as a plasticizer for EP, resulting in the lower T_gs.

In addition, tensile and impact strength tests are used to evaluate the mechanical properties of EP and EP/[Dmim]Tos. Fig. 4 shows their stress-strain curves and unnotched izod impact strength. The corresponding data are also listed in Table 1. Except the stress at break and Young modulus, the elongation at break and the impact strength of EP/[Dmim]Tos are almost as same as that of pure EP. Compared to pure EP, their stress at break has a little lower, however, their Young modulus are somewhat higher. Although the crosslinking density of EP/[Dmim]Tos is raised, dispersity and plasticization of the unreacted [Dmim]Tos cannot be neglected. On the whole, the mechanical properties of EP/[Dmim]Tos are maintained after the addition of [Dmim]Tos.

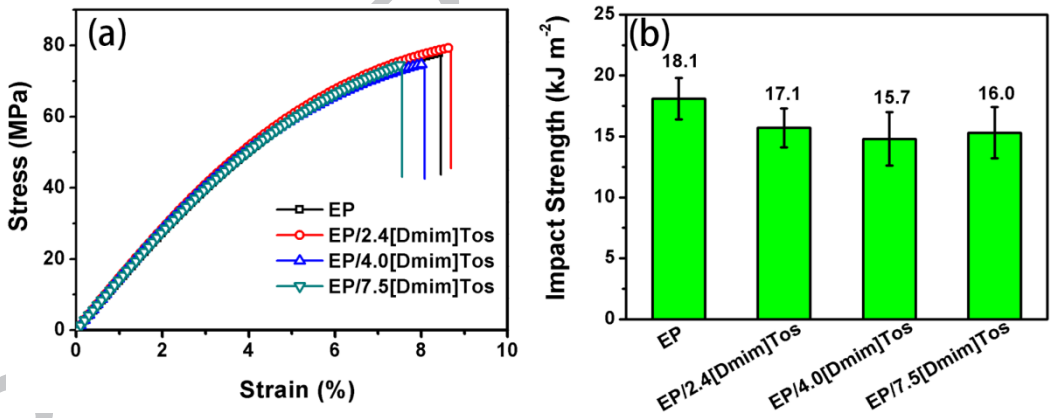

Fig. 4. Stress-strain curves (a) and unnotched izod impact strength (b) of EP and EP/[Dmim]Tos.

To further investigate the dispersion and compability between [Dmim]Tos and EP matrix, SEM and EDX element mapping was used to investigate the cryo-fractured surface of EP and EP/[Dmim]Tos (shown in Fig. 5). Compared with pure EP, the fractured surface of EP/[Dmim]Tos are slightly rough. In the the EDX elements mapping image, the phosphorus signal (P, in yellow) represents [Dmim]Tos,

while C signal (in red) is a representation of the epoxy matrix and the carbon atom derived from [Dmim]Tos. From the elements mapping image, we can see that phosphorus elements disperse very well in the carbon elements even for the sample containing 7.5 wt% [Dmim]Tos. This result indicates again that [Dmim]Tos has good compatibility with EP because of the participation of [Dmim]Tos in the curing process. Due to the good affinity with epoxy resin, the addition of small amount of [Dmim]Tos almost has no effect on the transparency of EP (shown in Fig. 5e). Only for EP/7.5[Dmim]Tos sample, its transparency is reduced.

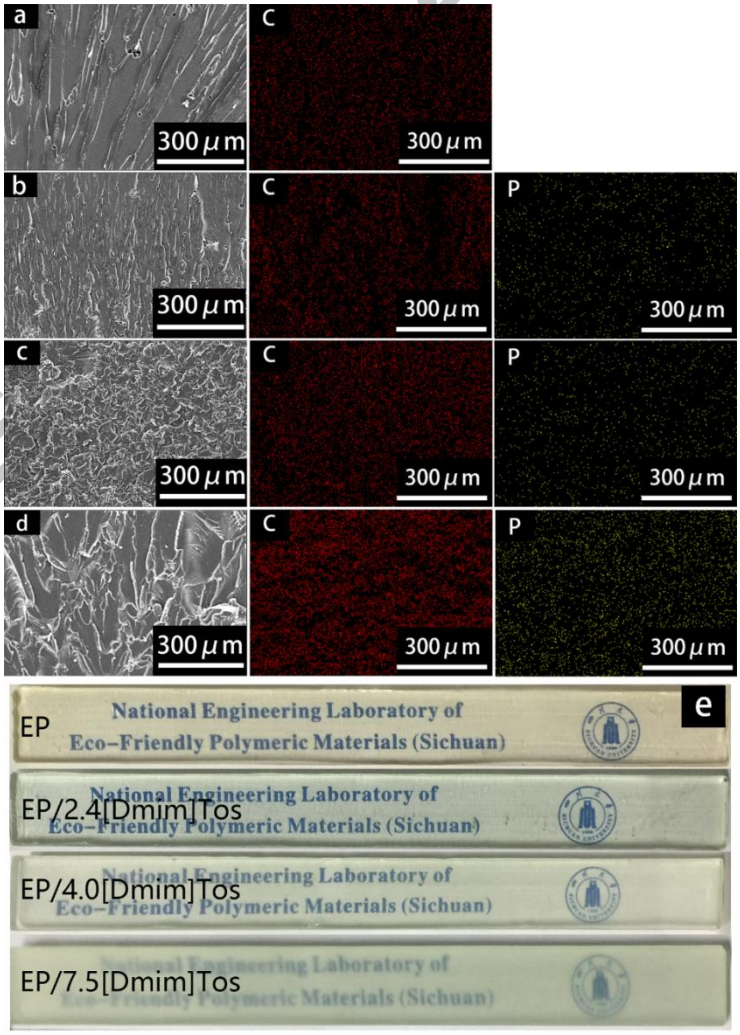

Fig. 5. SEM and elements mapping images (P in yellow signal and C in red signal) of EP (a),

EP/2.4[Dmim]Tos (b), EP/4.0[Dmim]Tos(c), EP/7.5[Dmim]Tos(d); and digital photographs of cured EP and EP/[Dmim]Tos (e).

3.3. Thermal stability of EP and EP/[Dmim]Tos

The thermal stability of EP/[Dmim]Tos is evaluated by TGA under nitrogen and air atmospheres. Fig. 6 shows the TG and DTG curves of EP and EP/[Dmim]Tos. The decomposition data obtained from Fig. 6, including the initial decomposition temperature, which is defined as the temperature at 5% weight loss ($T_{5\%}$), the temperature at maximum decomposition rate (T_{max}), as well as the residual mass at 700 °C (R_{700}) are summarized in Table 2, respectively.

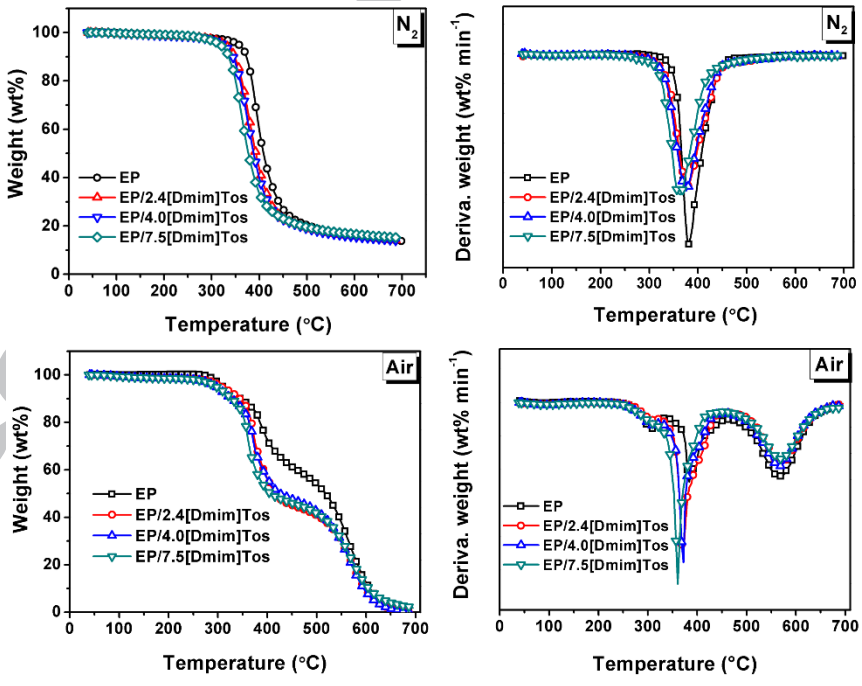

Fig. 6. TG and DTG curves of cured EP and EP/[Dmim]Tos under nitrogen (a and b) or air (c and d) atmospheres.

In nitrogen atmosphere, there is only one decomposition region for all samples. Compared to pure EP, the $T_{5\%}$s of cured EP/[Dmim]Tos decrease. From the TG and DTG curves of [Dmim]Tos (Fig. S3), we can find that [Dmim]Tos has lower $T_{5\%}$ in nitrogen and air atmosphere (298 °C and 187.4 °C, respectively). So, the addition of [Dmim]Tos makes EP present lower initial decomposition temperature. The T_{max}s of EP/[Dmim]Tos decrease obviously compared with that of EP. This illustrates that the decomposition of EP is accelerated by the organic phosphorus compounds released from [Dmim]Tos.

Under air atmosphere, the thermogravimetric curves of EP exhibit two stages decomposition. The first stage attributes to the degradation of epoxy chains, and the second one corresponds to the decomposition between char residue and oxygen [46]. Compared to pure EP, the $T_{5\%}$s, T_{max1}s of EP/[Dmim]Tos are reduced slightly, which means EP/[Dmim]Tos maintains good thermal stability in the air atmosphere. Additionally, the T_{max2}s of EP/[Dmim]Tos are little higher than EP. In terms of R_{700} values of EP/[Dmim]Tos, they decrease first and then increase with the increase of [Dmim]Tos. The above results indicate the addition of [Dmim]Tos promotes the decomposition of EP in the initial decomposition process, which is caused by some phosphorus-based acids or sulfur-based acid generated from [Dmim]Tos decomposition. While in the following decomposition process, these acids can act as dehydrating agents for the formation of stable char layers [47].

Table 2 Thermal decomposition data for cured EP and EP/[Dmim]Tos.

Samples	Nitrogen			Air			
	$T_{5\%}$[a] (℃)	T_{max}[b] (℃)	R_{700}[d] (wt%)	$T_{5\%}$ (℃)	T_{max1} (℃)	T_{max2} (℃)	R_{700} (wt%)
EP	356.9	393.0	13.7	310.1	382.8	565.4	1.75
EP/2.4[Dmim]Tos	328.2	378.9	13.9	308.2	370.7	563.6	0.05
EP/4.0[Dmim]Tos	323.6	375.6	13.8	296.2	371.4	569.0	0.15
EP/7.5[Dmim]Tos	317.5	363.5	15.1	297.1	360.3	568.2	1.83

a: The temperature at 5% weight loss; b: The temperature at maximum decomposition rate; d: The residual mass at 700 ℃.

3.4. Flame retardancy of cured EP/[Dmim]Tos

The flame retardant performance of [Dmim]Tos for EP is investigated by LOI and UL-94 tests, the obtained data are shown in Table 3. The LOI value of the EP is only 26.5%, and the LOI values of EP/[Dmim]Tos increase significantly with the increase of [Dmim]Tos content. Detailedly, the LOI value for EP/2.4[Dmim]Tos with phosphorus content of 0.12% is as high as 31.7. Further increasing the [Dmim]Tos amount, EP/7.5[Dmim]Tos can acquire the LOI value of 33.9%. In the UL-94 test, EP is no rating. However, the EP/4.0[Dmim]Tos, with only 0.2 wt% phosphorus content, can pass the V-0 level. During the UL-94 test, we find that the flame is blown out by the airflows released from the surface of the matrix. This phenomenon is also observed by other researchers when some phosphorus-containing flame retardants are used [50-52]. Compared with the other flame retardants used in EP, [Dmim]Tos shows excellent flame retardant efficiency for EP [7, 50, 53].

Table 3 LOI and UL-94 results for cured EP and EP/[Dmim]Tos.

Samples	[Dmim]Tos content (wt.%)	P content (wt.%)	LOI (%)	UL-94	
				t_1/t_2[a]	Ratings
EP	0	0	26.5	>1min/-	NR[b]
EP/2.4[Dmim]Tos	2.4	0.12	31.7	23s/3s	V-1
EP/4.0[Dmim]Tos	4.0	0.20	32.5	2s/2s	V-0
EP/7.5[Dmim]Tos	7.5	0.36	33.9	1s/2s	V-0

a: Average burning time after the 10 s ignition; b: No rating.

To further study the combustion behavior of the cured EP and EP/[Dmim]Tos, the cone calorimeter test is introduced. The curves of heat release rate (HRR), total heat release (THR), smoke production rate (SPR), total smoke production (TSR) are shown in Fig. 7. The corresponding data are given in Table 4. The neat EP burns rapidly after ignition and the peak heat release rate (*p*-HRR) is 1125.8 kW/m^2. When 4 wt% [Dmim]Tos is added into EP, the *p*-HRR value of EP/4.0[Dmim]Tos drops to 705.4 kW/m^2, which is reduced by 37% compared with EP. Moreover, the average effective heat of combustion (av-EHC), THR and TSR values of EP/[Dmim]Tos decrease compared with pure EP, indicating [Dmim]Tos plays an important role in the combustion suppression of EP. However, the time to ignition (TTI) of EP/[Dmim]Tos is lower than EP, which is mainly because of the early decomposition of [Dmim]Tos. Although the average CO yields (av-COY) of EP/[Dmim]Tos gradually increase with the increase content of [Dmim]Tos, their values are almost as same as that of EP. Also, the average CO_2 yields (av-CO_2Y) of EP/[Dmim]Tos are a little lower than EP. These results mean that [Dmim]Tos suppresses the combustion of EP, at the same time it does not aggravate the smoke release especially CO yields.

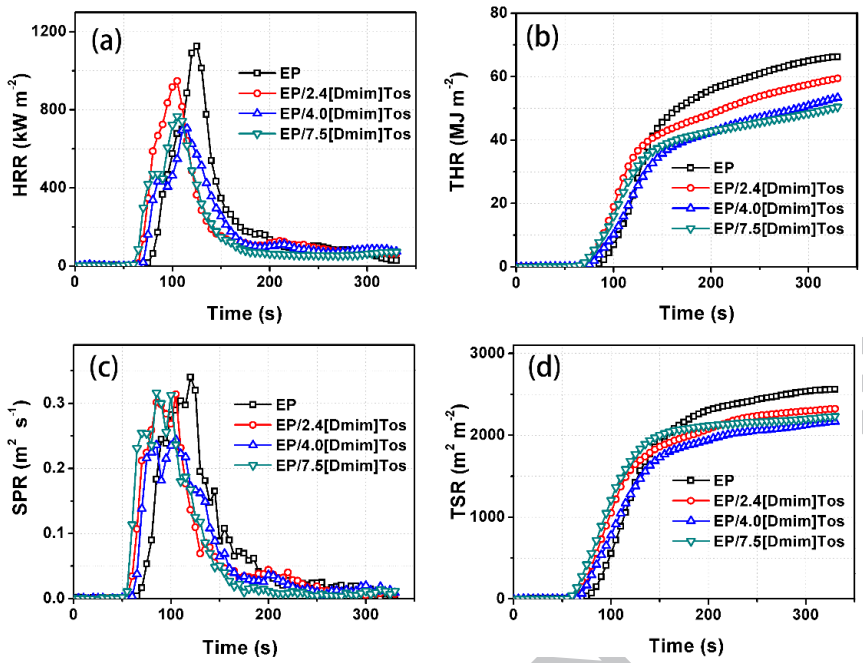

Fig. 7. Heat release rate (a), total heat release (b), smoke production rate (c), and total smoke release (d) curves of EP and EP/[Dmim]Tos.

Table 4 Cone calorimeter results of EP and EP/[Dmim]Tos.

Samples	TTI (s)	*p*-HRR ($kW \cdot m^{-2}$)	THR ($MJ \cdot m^{-2}$)	av-EHC ($MJ \cdot kg^{-1}$)	TSR ($m^2 \cdot m^{-2}$)	av-COY ($kg \cdot kg^{-1}$)	av-CO_2Y ($kg \cdot kg^{-1}$)
EP	61	1125.8	66.2	22.8	2561	0.071	1.942
EP/2.4[Dmim]Tos	51	947.6	67.3	22.5	2379	0.084	1.997
EP/4.0[Dmim]Tos	57	705.4	57.6	21.4	2215	0.095	1.841
EP/7.5[Dmim]Tos	51	767.0	56.2	20.1	2269	0.100	1.790

3.5. Analysis on char residue

To evaluate the morphology of the char residues after cone calorimeter test, digital camera and scanning electron microscope (SEM) have been used. Fig. S4 exhibits the digital photos of char residue for EP and EP/[Dmim]Tos thermosets after cone calorimeter test. From Fig. S4, we can see that there are a small amount of fragmentary char left for pure EP. Compared to EP, the char residue of EP/[Dmim]Tos

are more continuous and compact.

The SEM images of EP, EP/[Dmim]Tos char residue are presented in Fig. 8, and their microstructure can be seen clearly. The char residue of neat EP displays discontinuous structure in the exterior surface, and shows many tiny holes in the interior surface after combustion. However, from the exterior surfaces of the char layer for EP/[Dmim]Tos, they show compact carbon layer, especially for EP/7.5[Dmim]Tos. In the interior surfaces of EP/[Dmim]Tos, except EP/2.4[Dmim]Tos, the char layer of other samples becomes continuous, and some honeycombed structure can be observed for EP/4.0[Dmim]Tos and EP/7.5[Dmim]Tos. The compact char layer plays an important role in the combustion suppression, which can effectively isolate oxygen and heat, as well as prevent further decomposition of the substrate. The above results indicate [Dmim]Tos has the ability to catalyze char formation of EP and flame retard EP.

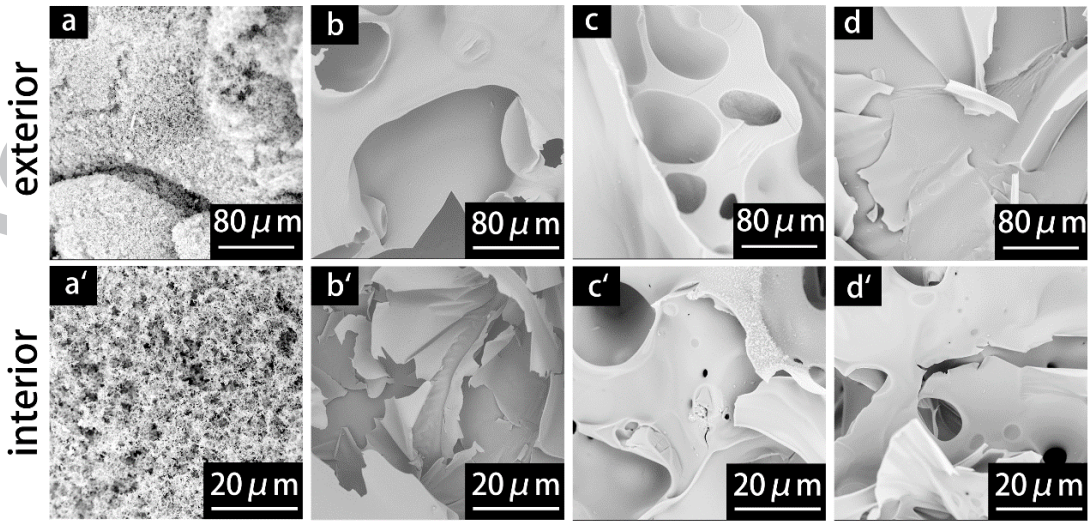

Fig. 8. SEM images of the char residues of EP (a, a′), EP/2.4[Dmim]Tos (b,b′), EP/4.0[Dmim]Tos (c,c′), EP/7.5[Dmim]Tos (d,d′) after cone calorimeter test.

Raman spectroscopy is an effective tool to analyze the degree of structural graphitization of carbonaceous material (Fig. 9). As shown in Fig. 9, there are two remarkable peaks at 1360 cm^{-1} and 1590 cm^{-1} in spectra, which belong to the D and G band, respectively. Generally, D band corresponds to the unordered carbon in the char residue, which represents the vibration of the carbon atoms in the disordered graphite structure. G band is related to the sp^2-bonds carbon structure in graphite layers, and corresponds to the organized carbon. So the ratio of integrated intensities (I_D/I_G) can be used to estimate the graphitization of the char residue. The graphitization increases as the ratio of I_D/I_G decreases [54]. It is found that the I_D/I_G values for EP/[Dmim]Tos are lower than that of EP, indicating that the addition of [Dmim]Tos increases the graphitization of the char residue of EP. This result is also in accordance with the SEM results.

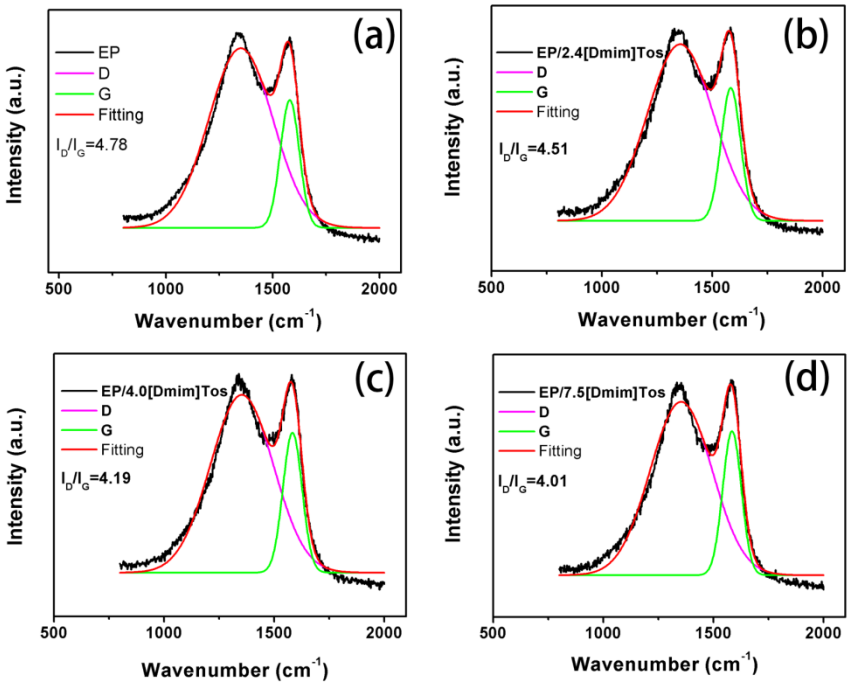

Fig. 9. Raman spectra of char residues of EP (a), EP/2.4[Dmim]Tos (b) EP/4.0[Dmim]Tos (c), EP/7.5[Dmim]Tos after cone calorimeter test.

To investigate the detailed chemical component of the residue, XPS analysis of the char residue for EP and EP/[Dmim]Tos after cone calorimetric test is applied. Fig. 10 shows the C_{1s} spectra, and the detailed data of C_{1s} chemical bonds are given in Table 5. N_{1s}, O_{1s}, and P_{2p} spectra are illustrated in Fig. S5. The ratios of the relative element concentration obtained from the integral of deconvolution spectra are shown in Table S1. As shown in Fig. 10, there are four binding states from C_{1s} spectra for all samples. The peaks at 284.4 and 284.8 eV belong to the C-H, C-C and C=C bonds in aliphatic and aromatic components. In addition, the peak at 285.4 eV is ascribed to the C-O-C and C-OH bonds. The signal of the C=O bond appears at 287.2 eV. The signal at 289.9 eV is assigned to COOR groups. These peaks are mainly related to the structure produced by dehydration and carbonization during combustion [55]. C_{ox} stands for the oxidized carbons, while C_a denotes the aliphatic and aromatic carbons. According to the literature, the value of C_{ox}/C_a can represent the percentage of aromatic hydrocarbons in char residue [56]. The smaller value of C_{ox}/C_a signifies the bigger condensation degree of the aromatic species. From Table 5, we can see that the C_{ox}/C_a values of EP/[Dmim]Tos decrease compared with that of EP. This means [Dmim]Tos can make EP/[Dmim]Tos produce more aromatic hydrocarbons in the char after the combustion process, which has a positive contribution to the flame retardant process. But the C_{ox}/C_a values of EP/[Dmim]Tos are not further reduced

when [Dmim]Tos content is raised, implying that its promotion effect on aromatic hydrocarbons formation is limited.

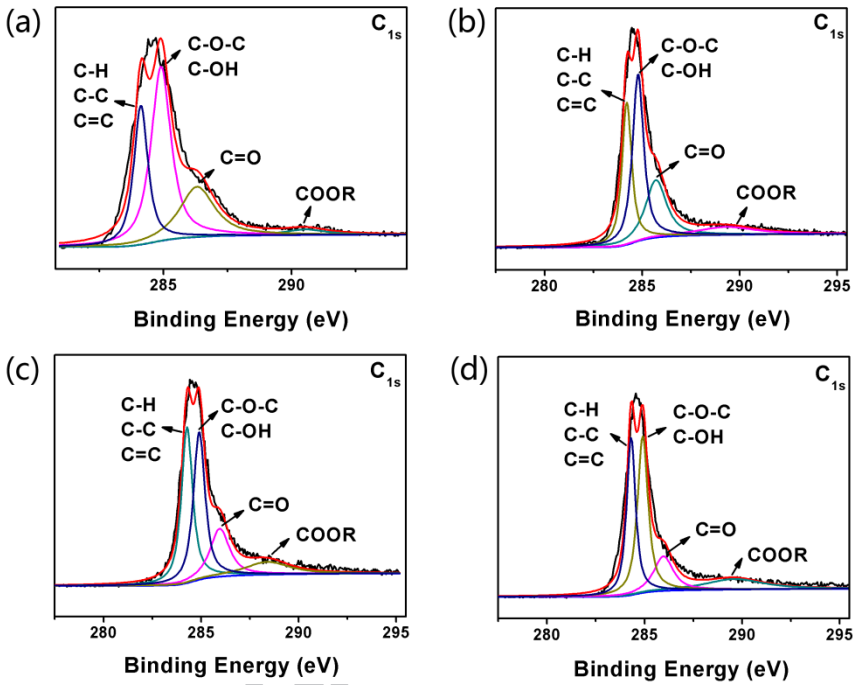

Fig. 10. C_{1s} spectra of residual char after cone calorimeter test for (a) EP, (b) EP/2.4[Dmim]Tos, (c) EP/4.0[Dmim]Tos, (d)EP/7.5[Dmim]Tos.

Table 5 C_{1s} XPS data of different chemical bonds for EP and EP/[Dmim]Tos.

Sample	C-C C-H C=C area (%)	C-O-C C-OH area (%)	C=O area (%)	COOR area (%)	C_{ox}/C_a
EP	33	26	21	20	2.03
EP/2.4[Dmim]Tos	42	23	18	17	1.17
EP/4.0[Dmim]Tos	46	20	17	17	1.27
EP/7.5[Dmim]Tos	44	22	17	17	1.38

C_{ox}: oxidized carbons. C_a: aliphatic and aromatic carbons.

In Fig. S5, there are two peaks at 398.6 eV and 400 eV in N_{1s} spectra, which can be ascribed to C-N and C=N bonds, respectively. As shown in Table S1, the nitrogen

element weight ratio of char residue for EP/[Dmim]Tos is lower than EP, meaning more nitrogen elements have been released during combustion. Two peaks at 530.8 eV (attributed to C=O bond) 532.9 eV (assigned to C-O-C or C-OH bonds) can be observed in O_{1s} spectra. It is noteworthy that the content of oxygen element in EP/[Dmim]Tos is higher than that of EP, indicating that EP/[Dmim]Tos can maintain more oxygen atoms after combustion. Besides, there are two peaks at 132.5 eV and 133.7 eV in P_{2p} spectra, which are assigned to the P-O-C or PO_3 groups and P_2O_5 derivatives, respectively. These peaks demonstrate that [Dmim]Tos can produce polyphosphonate or pyrophosphate during the combustions [57], which can catalyze dehydration and carbonation of EP.

3.6. Gaseous products analysis

To better understand the flame retarding mechanism of EP/[Dmim]Tos, gas phase function is also investigated. Therefore, the pyrolysis products of EP and EP/7.5[Dmim]Tos are analyzed by Py-GC/MS. The total ion chromatograms of EP and EP/7.5[DmimTos] are shown in Fig. 11. The corresponding peaks and their possible assignments are summarized in Table S2-S3.

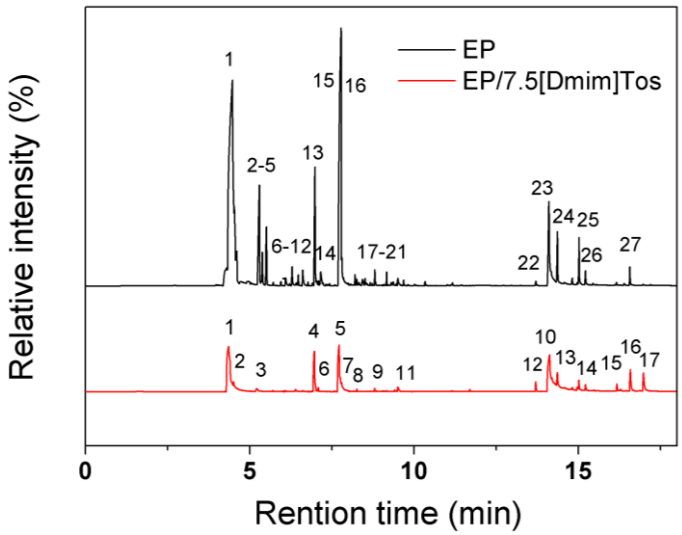

Fig. 11. Total ion chromatograms of EP and EP/7.5[Dmim]Tos.

As shown in Table S2, the main pyrolytic products of EP are phenol, benzofuran and bisphenol-A compounds, which are the fragments produced by the decomposition of epoxy polymers. The appearance of phenylamine is ascribed to the pyrolysis of DDM. For EP/7.5[Dmim]Tos, its total ion chromatogram is more simplified compared to EP one, indicating fewer kinds of compounds detected, which means the combustibles species decrease. Besides some same compounds as EP, a number of specific compounds, such as o-phenylphenol and DOPO, can be found. According to the literature [57-59], DOPO can generate PO free radicals or phosphorus compound through further degradation. On one hand, the phosphorus compounds retained in the char residue, which often make the carbon layer containing more phosphorus element, can catalyze dehydration reaction of epoxy resin. The higher phosphorus content in the char residue of EP/[Dmim]Tos has been demonstrated by XPS results (Table S1). On the other hand, PO free radicals can quench H or O free radicals generated in combustion process. Therefore, the DOPO fragments play an important role in flame

retarding EP/7.5[Dmim]Tos both in gas and condensed phases.

Consequently, based on the above analysis of gas phase products and condensed phase for the char residues, it can be concluded that the flame retardant mechanism of [Dmim]Tos on EP is in bi-phase: the gas phase is mainly the quenching effect of phosphorus-based radicals, and the condensed phase is the dehydration of phosphorous fragments for epoxy polymers as the formation of more aromatic char layer (shown in Fig. 12). The combination of gas phase and condensed phase makes [Dmim]Tos show better flame retardant effect for EP.

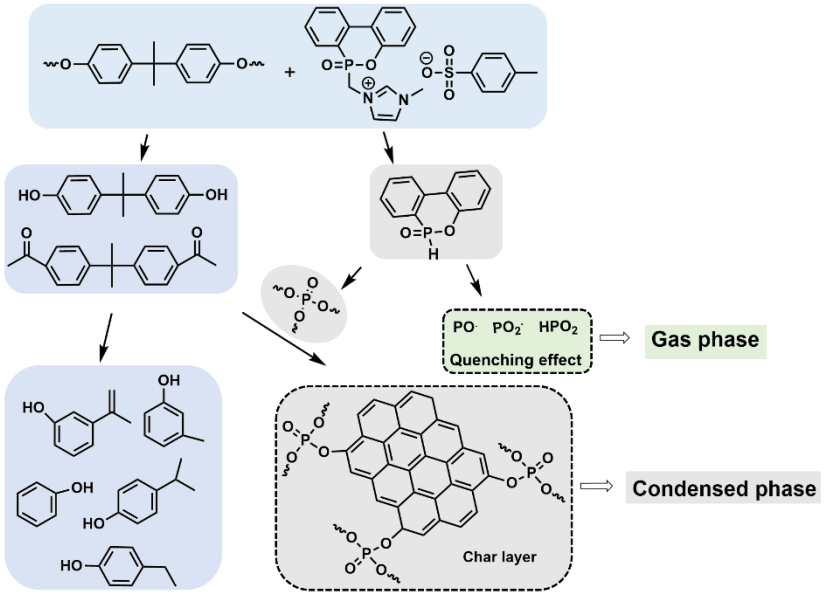

Fig. 12. Schematic illustration of the flame retardant mechanism of EP/[Dmim]Tos.

4. Conclusion

In this work, a novel N-methylimidazole sulfonate ionic liquid with DOPO structure, [Dmim]Tos, has been designed and prepared through the reaction of quaternization between N-methylimidazole and sulfonate. The cured EP and EP/[Dmim]Tos are

obtained in the presence of the curing agent DDM. It proves that [Dmim]Tos has promoting effect on the curing process of EP because of the acid and basic properties caused by the nitrogen atom in imidazole ring. When the amount of [Dmim]Tos is below 4.0 wt%, it almost has no effect on the transparency of EP. The addition of [Dmim]Tos basically maintains the mechanical properties of EP when its loading is lower than 7.5 wt%. Containing only 4.0 wt% [Dmim]Tos (phosphorus content of 0.2 wt%), EP/4.0[Dmim]Tos can pass UL-94 V-0 grade and obtain the LOI value of 32.5%. The *p*-HRR, av-EHC, THR and TSR values of EP/[Dmim]Tos decrese obviously compared with that of pure EP, indicating that [Dmim]Tos plays an important role in the combustion suppression of EP. Based on the analysis on the char residue and the pyrolysis products of EP/[Dmim]Tos, it can be deduced that the flame retardant effect of [Dmim]Tos on epoxy resin is both in condensed and gaseous phases. Due to the excellent flame retardant efficiency and the good affinity with EP, EP/4.0[Dmim]Tos owns higher fire safety and at the same time possesses good mechanical properties, transparency and thermal properties, which exhibits wider applications in the future.

Acknowledgements

This work was supported financially by the National Science Foundation of China (51573104 and 51721091), and the Sichuan Province Youth Science and Technology Innovation Team (No. 2017TD0006).

Supporting Information

^{1}H-NMR spectrum of DOPO-Tos, DSC curves of cured neat EP and EP/[Dmim]Tos, TG and DTG curves of [Dmim]Tos, Digital images of the char residues of EP (a, a′), EP/2.4[Dmim]Tos (b,b′), EP/4.0[Dmim]Tos (c,c′), EP/7.5[Dmim]Tos (d,d′) after cone calorimeter test, N_{1s}, O_{1s}, P_{1s} spectra of the char residues after cone calorimetry for (a) EP, (b) EP/2.4[Dmim]Tos, (c) EP/4.0[Dmim]Tos, (d)EP/7.5[Dmim]Tos, Relative element contents of the char residues of different samples after cone calorimeter test, Compounds identified in the pyrograms of EP, Compounds identified in the pyrograms of EP/7.5[Dmim]Tos.

References

[1] P. Cong, S. Chen, J. Yu, Investigation of the properties of epoxy resin-modified asphalt mixtures for application to orthotropic bridge decks, J. Appl. Polym. Sci. 121 (2011) 2310-2316.

[2] H. Gu, C. Ma, J. Gu, J. Guo, X. Yan, J. Huang, Q. Zhang, Z. Guo, An overview of multifunctional epoxy nanocomposites, J. Mater. Chem. C 4 (2016) 5890-5906.

[3] B. Tang, G. Hu, H. Gao, L. Hai, Application of graphene as filler to improve thermal transport property of epoxy resin for thermal interface materials, Int. J. Heat Mass Transfer 85 (2015) 420-429.

[4] G. Camino, G. Tartaglione, A. Frache, C. Manferti, P. Finocchiaro, L. Falqui, Combined Fire Retardant Action of Phosphonated Structures and Clay Dispersion in Epoxy Resin, ACS Symp. Ser. 922 (2005) 21-35.

[5] S.M. Unlu, S.D. Dogan, M. Dogan, Comparative study of boron compounds and aluminum trihydroxide as flame retardant additives in epoxy resin, Polym. Adv. Technol. 25 (2014) 769-776.

[6] S. Huo, J. Wang, S. Yang, B. Zhang, X. Chen, Q. Wu, L. Yang, Synthesis of a novel reactive flame retardant containing phosphaphenanthrene and piperidine groups and its application in epoxy resin, Polym. Degrad. Stab. 146 (2017) 250-259.

[7] S. Yang, J. Wang, S. Huo, M. Wang, J. Wang, Preparation and flame retardancy of a compounded epoxy resin system composed of phosphorus/nitrogen-containing active compounds, Polym. Degrad. Stab. 121 (2015) 398-406.

[8] J. Zhou, J.P. Lucas, Hygrothermal effects of epoxy resin. Part II: variations of glass transition temperature, Polymer 40 (1999) 5513-5522.

[9] B.S. Kim, Effect of cyanate ester on the cure behavior and thermal stability of epoxy resin, J. Appl. Polym. Sci. 65 (1997) 85-90.

[10] Y. Tan, Z.B. Shao, X.F. Chen, J.W. Long, L. Chen, Y.Z. Wang, Novel Multifunctional Organic-Inorganic Hybrid Curing Agent with High Flame-Retardant Efficiency for Epoxy Resin, ACS Appl. Mater. Interfaces 7 (2015) 17919-17928.

[11] Z.B. Shao, M.X. Zhang, Y. Li, Y. Han, L. Ren, C. Deng, A Novel Multi-functional Polymeric Curing Agent: Synthesis, Characterization, and Its Epoxy Resin with Simultaneous Excellent Flame Retardance and Transparency, Chem. Eng. J. 345 (2018) 471-482.

[12] S. Caporali, A. Fossati, A. Lavacchi, I. Perissi, A. Tolstogouzov, U. Bardi, Aluminium electroplated from ionic liquids as protective coating against steel corrosion, Corros. Sci. 50 (2008) 534-539.

[13] C. Maton, N. De Vos, C.V. Stevens, Ionic liquid thermal stabilities: decomposition mechanisms and analysis tools, Chem. Soc. Rev. 42 (2013) 5963-5977.

[14] R. Yuan, Y.j. Wang, Y. Fang, W.h. Ge, W. Lin, M.q. Li, J.b. Xu, Y. Wan, Y. Liu, H. Wu, The first direct synthesis of chiral Tröger's bases catalyzed by chiral glucose-containing pyridinium ionic

liquids, Chem. Eng. J. 316 (2017) 1026-1034.

[15] L. Zhang, J. Wang, Y. Sun, B. Jiang, H. Yang, Deep oxidative desulfurization of fuels by superbase-derived Lewis acidic ionic liquids, Chem. Eng. J. 328 (2017) 445-453.

[16] L. Miao, H. Duan, M. Liu, W. Lu, D. Zhu, T. Chen, L. Li, L. Gan, Poly(ionic liquid)-derived, N, S-codoped ultramicroporous carbon nanoparticles for supercapacitors, Chem. Eng. J. 317 (2017) 651-659.

[17] Y. Zhou, J. Qu, Ionic Liquids as Lubricant Additives: A Review, ACS Appl. Mater. Interfaces 9 (2017) 3209-3222.

[18] M. Rahman, C.S. Brazel, Ionic liquids: New generation stable plasticizers for poly(vinyl chloride), Polym. Degrad. Stab. 91 (2006) 3371-3382.

[19] N.V. Plechkova, K.R. Seddon, Applications of ionic liquids in the chemical industry, Chem. Soc. Rev. 37 (2008) 123-150.

[20] M. Yousfi, S. Livi, J. Duchet-Rumeau, Ionic liquids: A new way for the compatibilization of thermoplastic blends, Chem. Eng. J. 255 (2014) 513-524.

[21] H. Khakan, S. Yeganegi, Molecular Dynamics Simulations of Amide Functionalized Imidazolium Bis(trifluoromethanesulfonyl)imide Dicationic Ionic Liquids, J. Phys. Chem. B 121 (2017) 7455-7463.

[22] M. Zavrel, D. Bross, M. Funke, J. Büchs, A.C. Spiess, High-throughput screening for ionic liquids dissolving (ligno-)cellulose, Bioresour. Technol. 100 (2009) 2580-2587.

[23] R.L. Wu, X.L. Wang, F. Li, H.Z. Li, Y.Z. Wang, Green composite films prepared from cellulose, starch and lignin in room-temperature ionic liquid, Bioresour. Technol. 100 (2009) 2569-2574.

[24] B. Yuan, J. Guan, J. Peng, G.z. Zhu, J.h. Jiang, Green hydrolysis of corncob cellulose into

5-hydroxymethylfurfural using hydrophobic imidazole ionic liquids with a recyclable, magnetic metalloporphyrin catalyst, Chem. Eng. J. 330 (2017) 109-119.

[25] H. Gui, P. Xu, Y. Hu, J. Wang, X. Yang, A. Bahader, Y. Ding, Synergistic effect of graphene and an ionic liquid containing phosphonium on the thermal stability and flame retardancy of polylactide, RSC Adv. 5 (2015) 27814-27822.

[26] K. Subramaniam, A. Das, L. Häußler, C. Harnisch, K.W. Stöckelhuber, G. Heinrich, Enhanced thermal stability of polychloroprene rubber composites with ionic liquid modified MWCNTs, Polym. Degrad. Stab. 97 (2012) 776-785.

[27] X. Yang, N. Ge, L. Hu, H. Gui, Z. Wang, Y. Ding, Synthesis of a novel ionic liquid containing phosphorus and its application in intumescent flame retardant polypropylene system, Polym. Adv. Technol. 24 (2013) 568-575.

[28] S. Chen, J. Li**,** Y. Zhu, Z. Guo, S. Su, Increasing the efficiency of intumescent flame retardant polypropylene catalyzed by polyoxometalate based ionic liquid, J. Mater. Chem. A 1 (2013) 15242-15246.

[29] F. Xiao, K. Wu, F. Luo, Y. Guo, S. Zhang, X. Du, Q. Zhu, M. Lu, An efficient phosphonate-based ionic liquid on flame retardancy and mechanical property of epoxy resin, J Mater Sci. 52 (2017) 13992-14003.

[30] M. Petkovic, K.R. Seddon, L.P. Rebelo, C. Silva Pereira, Ionic liquids: a pathway to environmental acceptability, Chem. Soc. Rev. 40 (2011) 1383-1403.

[31] Y.R. Ham, D.H. Lee, S.H. Kim, Y.J. Shin, M. Yang, J.S. Shin, Microencapsulation of imidazole curing agent for epoxy resin, J. Ind. Eng. Chem. 16 (2010) 728-733.

[32] Q.X. He, L. Tang, T. Fu, Y.Q. Shi, X.L. Wang, Y.Z. Wang, Novel phosphorus-containing

halogen-free ionic liquids: effect of sulfonate anion size on physical properties, biocompatibility, and flame retardancy, RSC Adv. 6 (2016) 52485-52494.

[33] Y. Cao, X.L. Wang, W.Q. Zhang, X.W. Yin, Y.Q. Shi, Y.Z. Wang, Bi-DOPO Structure Flame Retardants with or without Reactive Group: Their Effects on Thermal Stability and Flammability of Unsaturated Polyester, Ind. Eng. Chem. Res. 56 (2017) 5913-5924.

[34] W. Zhang, X. Li, R. Yang, Study on flame retardancy of TGDDM epoxy resins loaded with DOPO-POSS compound and OPS/DOPO mixture, Polym. Degrad. Stab. 99 (2014) 118.

[35] X. Wang, Y. Hu, L. Song, W. Xing, H. Lu, P. Lv, G. Jie, Flame retardancy and thermal degradation mechanism of epoxy resin composites based on a DOPO substituted organophosphorus oligomer, Polymer 51 (2010) 2435-2445.

[36] J.Y. Shieh, C.S. Wang, Synthesis of novel flame retardant epoxy hardeners and properties of cured products, Polymer 42 (2001) 7617-7625.

[37] S. Yang, J. Wang, S. Huo, L. Cheng, M. Wang, Preparation and flame retardancy of an intumescent flame-retardant epoxy resin system constructed by multiple flame-retardant compositions containing phosphorus and nitrogen heterocycle, Polym. Degrad. Stab. 119 (2015) 251-259.

[38] K. Arimitsu, S. Fuse, K. Kudo, M. Furutani, Imidazole derivatives as latent curing agents for epoxy thermosetting resins, Mater. Lett. 161 (2015) 408-410.

[39] S. Xing, J. Yang, Y. Huang, Q. Zheng, J. Zeng, Preparation and characterization of a novel microcapsule-type latent curing agent for epoxy resin, Mater. Des. 85 (2015) 661-670.

[40] H. Mąka, T. Spychaj, W. Sikorski, Deep Eutectic Ionic Liquids as Epoxy Resin Curing Agents, Int. J. Polym. Anal. Charact. 19 (2014) 682-692.

[41] B.G. Soares, S. Livi, J. Duchet-Rumeau, J.F. Gerard, Synthesis and Characterization of

Epoxy/MCDEA Networks Modified with Imidazolium-Based Ionic Liquids, Macromol. Mater. Eng. 296 (2011) 826-834.

[42] M.S. Fedoseev, M.S. Gruzdev, L.F. Derzhavinskaya, 1-Butyl-3-methylimidazolium Salts as New Catalysts to Produce Epoxy-anhydride Polymers with Improved Properties, Int. J. Polym. Sci. 2014 (2014) 1-8.

[43] P.J. Flory, Principles of Polymer Chemistry, Cornell University Press, New York, 1953 Chapter XI.

[44] B. Francis, S. Thomas, R. Sadhana, N. Thuaud, R. Ramaswamy, S. Jose, V.L. Rao, Diglycidyl ether of bisphenol-A epoxy resin modified using poly(ether ether ketone) with pendent tert-butyl groups, J. Polym. Sci., Part B: Polym. 45 (2007) 2481-2496.

[45] X. Zhang, X. Yan, J. Guo, Z. Liu, D. Jiang, Q. He, H. Wei, H. Gu, H.A. Colorado, X. Zhang, S. Wei, Z. Guo, Polypyrrole doped epoxy resin nanocomposites with enhanced mechanical properties and reduced flammability, J. Mater. Chem. C 3 (2015) 162-176.

[46] J. Wang, C. Ma, P. Wang, S. Qiu, W. Cai, Y. Hu, Ultra-low phosphorus loading to achieve the superior flame retardancy of epoxy resin, Polym. Degrad. Stab. 149 (2018) 119-128.

[47] Y.J. Xu, J. Wang, Y. Tan, M. Qi, L. Chen, Y.Z. Wang, A novel and feasible approach for one-pack flame-retardant epoxy resin with long pot life and fast curing, Chem. Eng. J. 337 (2018) 30-39.

[48] W.J. Liang, B. Zhao, C.Y. Zhang, R.K. Jian, D.-Y. Liu, Y.Q. Liu, Enhanced flame retardancy of DGEBA epoxy resin with a novel bisphenol-A bridged cyclotriphosphazene, Polym. Degrad. Stab. 144 (2017) 292-303.

[49] S. Huo, J. Wang, S. Yang, J. Wang, B. Zhang, B. Zhang, X. Chen, Y. Tang, Synthesis of a novel phosphorus-nitrogen type flame retardant composed of maleimide, triazine-trione, and phosphaphenanthrene and its flame retardant effect on epoxy resin, Polym. Degrad. Stab. 131 (2016)

106-113.

[50] P. Wang, Z. Cai, Highly efficient flame-retardant epoxy resin with a novel DOPO-based triazole compound: Thermal stability, flame retardancy and mechanism, Polym. Degrad. Stab. 137 (2017) 138-150.

[51] W. Zhang, X. Li, R. Yang, Blowing-out effect in epoxy composites flame retarded by DOPO-POSS and its correlation with amide curing agents, Polym. Degrad. Stab. 97 (2012) 1314-1324.

[52] W. Zhang, X. Li, L. Li, R. Yang, Study of the synergistic effect of silicon and phosphorus on the blowing-out effect of epoxy resin composites, Polym. Degrad. Stab. 97 (2012) 1041-1048.

[53] P. Wang, L. Xia, R. Jian, Y. Ai, X. Zheng, G. Chen, J. Wang, Flame-retarding epoxy resin with an efficient P/N/S-containing flame retardant: Preparation, thermal stability, and flame retardance, Polym. Degrad. Stab. 149 (2018) 69-77.

[54] R. Sonnier, L. Dumazert, S. Livi, T.K.L. Nguyen, J. Duchet-Rumeau, H. Vahabi, P. Laheurte, Flame retardancy of phosphorus-containing ionic liquid based epoxy networks, Polym. Degrad. Stab. 134 (2016) 186-193.

[55] B. Yu, Y. Shi, B. Yuan, S. Qiu, W. Xing, W. Hu, L. Song, S. Lo, Y. Hu, Enhanced thermal and flame retardant properties of flame-retardant-wrapped graphene/epoxy resin nanocomposites, J. Mater. Chem. A 3 (2015) 8034-8044.

[56] S. Bourbigot, M. Le Bras, L. Gengembre, R. Delobel, XPS study of an intumescent coating application to the ammonium polyphosphate/pentaerythritol fire-retardant system, Appl. Surf. Sci. 81 (1994) 299-307.

[57] L. Qian, L. Ye, Y. Qiu, S. Qu, Thermal degradation behavior of the compound containing phosphaphenanthrene and phosphazene groups and its flame retardant mechanism on epoxy resin,

Polymer 52 (2011) 5486-5493.

[58] D. Shen, Y.J. Xu, J.W. Long, X.H. Shi, L. Chen, Y.Z. Wang, Epoxy resin flame-retarded via a novel melamine-organophosphinic acid salt: Thermal stability, flame retardance and pyrolysis behavior, J. Anal. Appl. Pyrolysis. 128 (2017) 54-63.

[59] M. Rakotomalala, S. Wagner, M. Doring, Recent Developments in Halogen Free Flame Retardants for Epoxy Resins for Electrical and Electronic Applications, Materials 3 (2010) 4300-4327.

Figure and Table Captions

Scheme 1. Synthetic route for [Dmim]Tos and 3D structure of [Dmim]Tos obtained by Chembio 3D MM2 Minimize Energy.

Fig. 1. ^{1}H-NMR (a), ^{13}C- NMR (b), ^{31}P-NMR (c) spectra of [Dmim]Tos.

Fig. 2. DSC heating scans of EP and EP/[Dmim]Tos (a), and the consumption of EP at different loading of [Dmim]Tos (b).

Fig. 3. DMA curves of EP and EP/[Dmim]Tos.

Fig. 4. Stress-strain curves (a) and unnotched izod impact strength (b) of EP and EP/[Dmim]Tos.

Fig. 5. SEM and elements mapping images (P in yellow signal and C in red signal) of EP (a), EP/2.4[Dmim]Tos (b), EP/4.0[Dmim]Tos(c), EP/7.5[Dmim]Tos(d); and digital photographs of cured EP and EP/[Dmim]Tos (e).

Fig. 6. TG and DTG curves of cured EP and EP/[Dmim]Tos under nitrogen (a and b) or air (c and d) atmospheres.

Fig. 7. Heat release rate (a), total heat release (b), smoke production rate (c), and total smoke release (d) curves of EP and EP/[Dmim]Tos.

Fig. 8. SEM images of the char residues of EP (a, a′), EP/2.4[Dmim]Tos (b,b′), EP/4.0[Dmim]Tos (c,c′), EP/7.5[Dmim]Tos (d,d′) after cone calorimeter test.

Fig. 9. Raman spectra of char residues of EP (a), EP/2.4[Dmim]Tos (b) EP/4.0[Dmim]Tos (c), EP/7.5[Dmim]Tos after cone calorimeter test.

Fig. 10. C_{1s} spectra of residual char after cone calorimeter test for (a) EP, (b) EP/2.4[Dmim]Tos, (c) EP/4.0[Dmim]Tos, (d)EP/7.5[Dmim]Tos.

Fig. 11. Total ion chromatograms of EP and EP/7.5[Dmim]Tos.

Fig. 12. Schematic illustration of the flame retardant mechanism of EP/[Dmim]Tos.

Table 1 Mechanical properties, T_g, and crosslinking density (v_e) of EP and EP/[Dmim]Tos.

Table 2 Thermal decomposition data for cured EP and EP/[Dmim]Tos.

Table 3 LOI and UL-94 results for cured EP and EP/[Dmim]Tos.

Table 4 Cone calorimeter results of EP and EP/[Dmim]Tos.

Table 5 C_{1s} XPS data of different chemical bonds for EP and EP/[Dmim]Tos.

Highlights

1. A novel ionic liquid containing DOPO and tosylate is synthesized.
2. [Dmim]Tos endows EP with excellent fire safety.
3. [Dmim]Tos has accelerating effect on the curing of EP .
4. Flame-retardant EP maintains its mechanical properties and transparency.

Graphical Abstract

Novel phosphorus-containing halogen-free ionic liquid toward fire safety epoxy resin with well-balanced comprehensive performance

Yue-Quan Shi, Teng Fu, Ying-Jun Xu, De-Fu Li, Xiu-Li Wang*, Yu-Zhong Wang

Center for Degradable and Flame-Retardant Polymeric Materials, College of Chemistry, State Key Laboratory of Polymer Materials Engineering, National Engineering Laboratory of Eco-Friendly Polymeric Materials (Sichuan), Sichuan University, Chengdu 610064, China.

*E-mail address: xiuliwang1@163.com

Fax: +86-28-85410755; Tel: +86-28-85410755